Uncertainty in Future High Flows in Qiantang River Basin, China

YE TIAN AND YUE-PING XU

Institute of Hydrology and Water Resources, Department of Civil Engineering, Zhejiang University, Hangzhou, Zhejiang, China

MARTIJN J. BOOIJ

Department of Water Engineering and Management, Faculty of Engineering Technology, University of Twente, Enschede, Netherlands

GUOQING WANG

State Key Laboratory of Hydrology-Water Resources and Hydraulic Engineering, Nanjing Hydraulic Research Institute, Nanjing, China

(Manuscript received 7 August 2013, in final form 27 June 2014)

ABSTRACT

Uncertainties in high flows originating from greenhouse gas emissions scenarios, hydrological model structures, and their parameters for the Jinhua River basin, China, were assessed. The baseline (1961–90) and future (2011–40) climates for A1B, A2, and B2 scenarios were downscaled from the general circulation model (GCM) using the Providing Regional Climates for Impacts Studies (PRECIS) regional climate model with a spatial resolution of 50 km × 50 km. Bias-correction methods were applied to the PRECIS-derived temperature and precipitation. The bias-corrected precipitation and temperature were used as inputs for three hydrological models [modèle du Génie Rural à 4 paramètres Journalier (GR4J), Hydrologiska Byråns Vattenbalansavdelning (HBV), and Xinanjiang] to simulate high flows. The parameter uncertainty was considered and quantified in the hydrological model calibration by means of the generalized likelihood uncertainty estimation (GLUE) method for each hydrological model for the three emissions scenarios. It was found that, compared with the high flows in the baseline period, the high flows in the future tended to decrease under scenarios A1B, A2, and B2. The largest uncertainty was observed in HBV, and GR4J had the smallest uncertainty. It was found that the major source of uncertainty in this study was from parameters, followed by the uncertainties from the hydrological model structure, and the emissions scenarios have the smallest uncertainty contribution to high flows in this study.

1. Introduction

Water resources are of key importance to human society and are also vulnerable to climate change. In recent years, climate change has changed water availability, accelerated floods and droughts, increased frequency of heavy precipitation events, and raised sea levels (Houghton et al. 2001). The impacts are occurring and are expected to continue in many regions of the world (Pachauri and Reisinger 2007). Therefore, investigating the impact of climate change on hydrology and water resources has become more important in recent decades (Bauwens et al. 2011; Zhang et al. 2011; Kerkhoven and Gan 2013; Tian et al. 2013). However, there are many sources of uncertainty in climate change impact analysis, bringing a big challenge to current water management under climate change (New and Hulme 2000; Refsgaard et al. 2006; Xu et al. 2013). In general, the uncertainty in simulating future discharges under climate change is mainly from the global climate models (GCMs), emissions scenarios, downscaling methods, hydrological models, and their parameters. Given the fact that these uncertainties cannot be reduced easily, it is necessary to investigate and quantify the uncertainties for robust decision making in water management under climate change.

Corresponding author address: Dr. Yue-Ping Xu, Institute of Hydrology and Water Resources, Department of Civil Engineering, Zhejiang University, Yuhangtang Road 388, Hangzhou, Zhejiang 310058, China.
E-mail: yuepingxu@zju.edu.cn; m.j.booij@utwente.nl

DOI: 10.1175/JHM-D-13-0136.1

The outputs from GCMs could be used to drive the hydrological models for large-scale hydrological applications. However, the spatial resolution of GCMs generally is too coarse since many hydrological models are applied to catchment scales, which require data with a higher resolution (Wigley et al. 1990). The mismatch between the spatial resolutions introduces uncertainty and cannot be neglected. There are generally two kinds of methods to downscale coarse-scale information of GCMs to the spatial scale of catchments, that is, statistical and dynamical downscaling (Wilby et al. 1998, 1999). Statistical downscaling is based on established empirical relationships between circulation indices at the large scale and predictive variables at the local scale. However, the results from statistical downscaling methods may not always be meteorologically consistent with GCMs. The advantage of dynamical downscaling is that it resolves atmospheric processes and is consistent with the GCMs (Wilby et al. 2002). Although differences in parameterizations, numerical techniques, vertical resolution, and even regional model domain may cause differences in results of regional climate models (RCMs), the downscaling uncertainty could be constrained by linking regional impacts to natural regime frequencies (Raje and Mujumdar 2010). RCMs have shown great advantages over GCMs in describing the regional climate variables, especially extreme climatic events (Bell et al. 2004).

Besides, different greenhouse gas emissions scenarios reflect different assumptions of the mode of development for the future. A number of studies have been carried out to investigate climate change impacts on discharges in many regions using different scenarios. Arnell (2003) used a macrohydrological model to study the effects of emissions scenarios on river runoff at a spatial resolution of $0.5° \times 0.5°$. The results indicated that the pattern of change in runoff is largely determined by simulated changes in precipitation. Similar results have also been obtained by other studies, which show that changes of runoff are proportional with the changes in rainfall (Boorman and Sefton 1997). Gosain et al. (2011) used a single scenario (A1B) and a single hydrological model [Soil and Water Assessment Tool (SWAT)] to quantify the impact of climate change on the water resources in India. The results show that despite the increase in precipitation, the water yields decreased with 30% for the near term and 50% for the long term. Driessen et al. (2010) used multiple scenarios (A1B, A2, and B1) and a single hydrological model [Hydrologiska Byråns Vattenbalansavdelning (HBV)] to study changes in discharge in the Ourthe catchment in Belgium. They found a decrease in summer and an increase in winter runoff for all scenarios. Most studies focused on applying different scenarios to a single hydrological model. Few studies have assessed model uncertainties under different scenarios. Jones et al. (2006) applied artificial scenarios to three lumped rainfall–runoff models for Australian catchments. They found out that the sensitivity of hydrological models is influenced by model structure and parameterization and runoff is about 3–5 times more sensitive to rainfall than to potential evapotranspiration. Najafi et al. (2011) moved a step forward by quantifying the uncertainty in different steps of the climate change impact assessment, using eight GCMs and four hydrological models under the A1B and B1 scenarios. The results indicated that the dominant uncertainty is from GCMs. They also emphasized that the differences in the changes between projected runoff in the future and the historical runoff are directly related to the choice of the GCM structure.

Another key source of uncertainty that cannot be neglected in water resources assessment is related to the hydrological models used, including model structure and parameters. Hydrologists used to search for an optimal parameter set through calibrating model parameters using observed catchment responses. However, the fact is that it is not possible to assume an optimum model structure or an optimum set of parameters that could represent many situations in reality, and the uncertainty of parameters should be considered when assessing the uncertainty in hydrological prediction (Beven 2006). More recently, various methods concerned with uncertainty in parameter estimation have been proposed and extensively used, such as generalized likelihood uncertainty estimation (GLUE; Beven and Binley 1992) and Markov chain Monte Carlo (MCMC; Vrugt et al. 2003). They are both Monte Carlo–based methods for estimating the model uncertainties. Besides, uncertainties from different sources could be combined by the Bayesian model averaging (BMA) approach (Raftery et al. 2005; Parrish et al. 2012) by assigning weights to the sources. The GLUE method represents an extension of Bayesian theory by using an informal likelihood measure to avoid overconditioning in dealing with uncertainty estimation (Beven et al. 2000). This is a remarkable aspect of the GLUE method and also the major difference with the Bayesian approach (Jin et al. 2010).

In many hydrological studies related to the uncertainty of climate change impacts, different GCMs, downscaling methods, and hydrological models have been used to estimate the changes and uncertainties of discharges for different emissions scenarios. However, some of them used the combination of a single scenario and a single rainfall–runoff model, some used multiple scenarios and a single rainfall–runoff model, and a few

have applied multiple scenarios and multiple rainfall–runoff models. To our knowledge, there is a very limited number of studies that incorporate the uncertainty from parameters of different rainfall–runoff models in assessing effects of uncertainties of climate change on hydrology. Kay et al. (2009) systematically estimated the flood frequency with uncertainty under climate change considering various sources of uncertainty (using four scenarios, five GCMs, eight RCMs, and two hydrological models). The results showed that the uncertainty from GCMs was generally larger than that related to emissions or hydrological models. However, the study was based on the single propagation of each source of uncertainty, and the propagation of multiple sources of uncertainty at once was not included. Furthermore, high flows have received much attention, as it is recognized that flooding often results in a great loss of human life and possession, and the damage is more serious in a densely populated region (Rebora et al. 2013). Much work has been done on the analysis of high flows under climate change in developed regions (Middelkoop et al. 2001; Booij 2005; Hannaford and Marsh 2008; Leander et al. 2008; Kay et al. 2009). However, relatively few studies were carried out for developing countries like China, and the uncertainties of high flows under climate change are less frequently studied compared to uncertainties in mean discharges. Therefore, we attempt to investigate uncertainties in high flows in a catchment in the east of China, where climate change may have considerable impacts on local hydrology (Xu et al. 2012).

In the present study, we put the emphasis on uncertainties in high flows in the near future (2011–40). Our aim is to assess to what extent emissions scenarios, hydrological models, and parameters exert impacts on high flows. The impacts of human activities such as reservoirs on high flows are not considered in this study in order to focus on climate change impact analysis. The research is carried out by using three emissions scenarios, three hydrological models, the GLUE method for estimation of parameter uncertainties, and the regional climate model Providing Regional Climates for Impacts Studies (PRECIS). The three scenarios A2, A1B, and B2 represent different temperature increases in the future, ranging from high to low, and different precipitation changes. The rainfall–runoff models we used have different numbers of parameters and different structures that represent the uncertainty in understanding the real physical processes. Uncertainties in high flows are propagated through emissions scenarios, hydrological models, and parameters. The study of uncertainties in high flows in the future can be supportive for water resources planning in the long term in eastern China and in China as a whole.

This paper is organized as follows. In section 2, a brief description of the hydrological and meteorological background of the case study area is provided, followed by an introduction of climate change scenarios, climate models, and hydrological models. Moreover, the bias-correction method and GLUE method are described. In section 3, the results of the study are shown, including the performance of the hydrological models, the effectiveness of the bias-correction method and the quantified uncertainties from the emissions scenarios, hydrological model structures and hydrological parameters. In section 4, the discussion of the results is given and in section 5 the conclusions from our analysis are drawn.

2. Methods

In this study, we focus on the annual maximum discharge with uncertainties from emissions scenarios, hydrological model structures, and parameters of the hydrological models. The proposed framework of the study is shown in Fig. 1. The uncertainty in scenarios is represented by the variability among scenarios A1B, A2, and B2. The uncertainty in hydrological model structures is represented by the variability among the modèle du Génie Rural à 4 paramètres Journalier (GR4J), HBV, and Xinanjiang models. The uncertainty in parameters of hydrological models is represented by behavioral parameter sets in 30 000 randomly selected parameter sets.

a. Study area

This study is carried out for Jinhua River basin, a subbasin of Qiantang River basin, which is the largest river in Zhejiang Province located in eastern China (Fig. 2). The origin of Jinhua River is in the higher mountain area that forms a natural boundary for the basin. Two tributaries, the Yiwu River and the Wuyi River, join in Jinhua city and form the Jinhua River. Finally, the Jinhua River flows northwest into the Qiantang River. The drainage area of the Jinhua River basin is 5996 km^2 and is characterized by a hilly landscape, so the floods come and go quickly after a rainfall event. The basin is dominated by a subtropical monsoon climate. The interseasonal variability of temperature and precipitation is large. There is abundant rainfall caused by the confrontation of the cold air from the north and warm air from the south, and another main cause is typhoons. The average annual precipitation is 1386 mm for the period of 1953–2008, with a minimum of 890 mm and a maximum of 1830 mm. The annual mean temperature is about 17°C. In winter, the lowest temperatures are below 0°C and the highest temperatures are up to 40°C in summer.

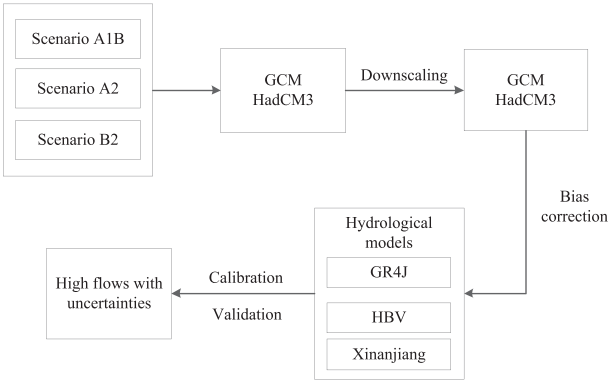

FIG. 1. The framework of the study.

Jinhua is one of the most densely populated and economically developed cities in Zhejiang Province. However, flooding is one of the most serious natural disasters in this region, which has posed a large threat to the safety of local people and their possessions (Wen et al. 2006). Our study is carried out for Jinhua River basin to assess the uncertainty of high flows under future climate change. The information of the observed data are listed in Table 1. Long-term observed daily data are available, including daily precipitation from 1961 to 1995 from five precipitation stations, daily temperature from 1961 to 1990 from a meteorological station, and daily discharge from 1981 to 1995 from the Jinhua hydrological station. The observed dataset is used for bias correction of the PRECIS output (1961–90), hydrological model calibration (1981–90), and model validation (1991–95). The potential evapotranspiration is estimated using the Hargreaves equation (Hargreaves and Samani 1983).

b. *Climate change scenarios*

Climate change scenarios are a set of images for the possible future based on different paths of economic development, which are used to assess the future vulnerability to climate change by projecting the greenhouse gas emissions. In 2000, the Intergovernmental Panel on Climate Change (IPCC) developed four different storylines (six emissions scenarios) to describe how the world might develop in the future, including population and economic growth patterns, energy consumption, and technological development (Nakićenović and Swart 2000). In this paper, we choose three scenarios from the IPCC report, which are A1B, A2, and B2, since these three scenarios are typical development modes. A1B describes a future world with very rapid economic growth based on a balanced technological change in the energy system. A2 describes a heterogeneous future world with increasing population and regionally oriented economic development. B2 describes a future world with continuously increasing population and intermediate levels of economic development.

c. *GCM and PRECIS*

Global climate models are often employed to estimate the impact of future greenhouse gas emissions scenarios on the global climate. However, GCMs have a coarse spatial resolution, usually about 200–300 km. To make a thorough assessment, more regional details of how future climate might change, including changes in variability and information on extreme events, are needed for impact analysis studies (Arnell et al. 2003).

The Hadley Centre Coupled Model, version 3 (HadCM3) is a coupled atmosphere–ocean GCM that has been widely used for climate prediction and sensitivity studies. It has 19 vertical levels with a horizontal resolution of 2.5° × 3.75°. The GCM was developed at the Hadley Centre and was described by Gordon et al. (2000).With the boundary conditions of HadCM3, the PRECIS RCM has been implemented for the A1B, A2, and B2 emissions scenarios. PRECIS has been used in many other regions in the world, including South Asia (Akhtar et al. 2008, 2009) and South America (Buytaert et al. 2010), and hence is used in this study. The PRECIS RCM is based on the atmospheric component of HadCM3 and is extensively described in Jones et al. (2004). The atmospheric dynamics module of PRECIS is a hydrostatic version of the full primitive equations and uses a regular longitude–latitude grid in the horizontal and a hybrid vertical coordinate. For this study, the PRECIS model domain has been set up with a horizontal resolution of 50 km × 50 km. The domain is roughly stretched over latitudes 28.15°–29.45°N and longitudes 119.15°–120.75°E. The PRECIS precipitation and computed potential evapotranspiration using projected temperature are used to drive the hydrological models for the baseline period 1961–90 and the future period 2011–40.

d. *Bias correction*

Model biases in RCMs may cause errors in outputs, which may bring uncertainty to hydrological simulations when climate data are used in hydrological models (Ueyama et al. 2010). Therefore, bias correction is necessary to match the RCM data with observed data. In our study, distribution-based scaling (DBS) is applied to adjust the future daily precipitation of PRECIS (Wood et al. 2002). It corrects the biases of both the frequency and intensity distribution of daily PRECIS precipitation for each month. It consists of two steps:

1) Correction of the precipitation frequency. Daily precipitation from the PRECIS model was truncated at a threshold based on its distribution. A threshold value is calculated based on the empirical observed

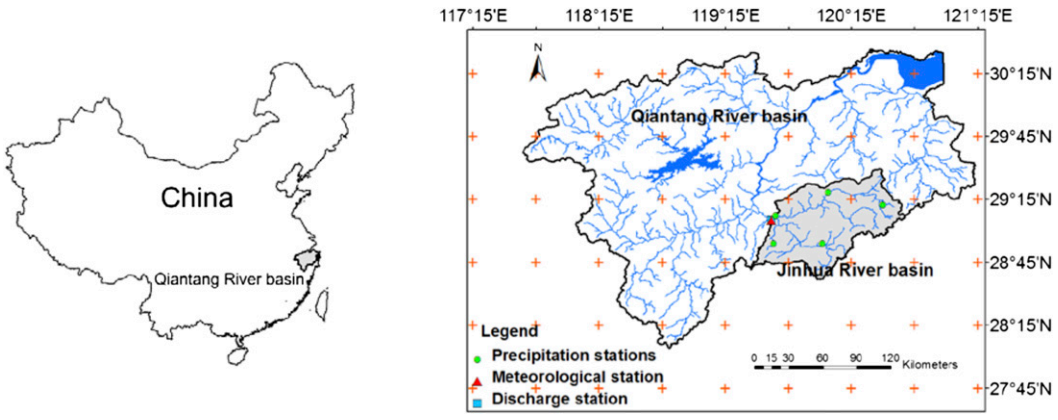

FIG. 2. The location of the study area and the distribution of the precipitation stations, meteorological station, and discharge station.

and PRECIS cumulative precipitation distribution as follows:

$$P_{\text{thr}} = F^{-1}_{\text{RCM}}[F_{\text{obs}}(P_{\text{obs}})], \tag{1}$$

where P_{thr} is the threshold value, P_{obs} is the minimum observed precipitation amount considered as a wet day (here we use 0.1 mm), $F_{\text{obs}}(\ldots)$ is the empirical cumulative distribution function of observed daily precipitation, and $F^{-1}_{\text{RCM}}(\ldots)$ is the inverse cumulative distribution function of RCM precipitation.

2) Correction of the precipitation intensity. One of the most commonly used distributions to describe the cumulative distribution function of precipitation intensities is the two-parameter gamma distribution. In this study, both observed and simulated precipitation intensity are represented by the gamma distribution. The bias-corrected precipitation can be calculated as follows:

$$P_{\text{cor}} = F^{-1}_{\text{obs}}[F_{\text{RCM}}(P_{\text{RCM}})], \tag{2}$$

where P_{cor} is the corrected daily precipitation, P_{RCM} is the truncated RCM precipitation, $F_{\text{RCM}}(\ldots)$ is the two-parameter cumulative distribution of truncated RCM precipitation, and $F^{-1}_{\text{obs}}(\ldots)$ is the inverse gamma cumulative distribution of observed data.

To correct the daily temperature, a different method is used. It adjusts the mean temperature of PRECIS by adding the difference between simulated and observed monthly mean temperature to the daily temperature in the corresponding month in the future. The corrected daily temperature was obtained as follows:

$$T_{\text{cor}} = T_{\text{RCM}} + (\overline{T}_{\text{obs}} - \overline{T}_{\text{RCM}}), \tag{3}$$

where T_{cor} is the corrected daily temperature, T_{RCM} is the daily temperature from PRECIS, $\overline{T}_{\text{obs}}$ is the observed monthly mean temperature, and $\overline{T}_{\text{RCM}}$ is the monthly mean temperature from PRECIS.

e. *Hydrological models*

There is a large variety of hydrological models with different levels of complexity, but no model is perfect in characterizing the real hydrological interactions. Models are supposed to be chosen according to the study region, basin characteristics, available data, and study purposes, but often the model selection is subject to the taste of the modeler and rarely is an objective model selection conducted (Najafi et al. 2011). In this study, we choose three lumped rainfall–runoff models of different complexities to study the hydrological response to climate change: GR4J, HBV, and Xinanjiang (Table 2).

GR4J, which contains four parameters with quick and slow flow components, was developed based on GR3J (Edijatno et al. 1999; Perrin et al. 2003). The four parameters of GR4J are the capacity of the production store, the groundwater exchange coefficient, the 1-day ahead capacity of the routing store, and the time base of the unit hydrograph. There are four submodels in GR4J: the soil moisture submodel, the effective precipitation submodel, the slow flow submodel, and the quick flow submodel. The total runoff is obtained by adding quick flow and slow flow together.

HBV was originally developed by the Swedish Meteorological and Hydrological Institute (SMHI; Bergström 1976, 1992; Lindström et al. 1997). HBV is composed of a precipitation and snow accumulation routine, a soil moisture routine, a quick runoff routine, a base flow routine, and a transformation function. HBV takes the effect of snow melting and accumulation into account.

TABLE 1. Information for precipitation, meteorological, and discharge stations.

		Lat (°N)	Lon (°E)	Time series	Duration (years)
Precipitation stations	Jinhua	29.08	119.62	1961–95	35
	Bada	29.20	120.50	1961–95	35
	Yiwu	29.30	120.07	1961–95	35
	Yongkang	28.90	120.02	1961–95	35
	Zhengzhai	28.90	119.63	1961–95	35
Meteorological station	Jinhua	29.08	119.62	1961–90	30
Discharge station	Jinhua	29.08	119.62	1981–95	15

However, in the study area it seldom snows in winter, and therefore snow accumulation and melting are not used. A linear function is used to calculate the actual evapotranspiration, which decreases as the soil moisture drops. Two types of runoff reservoirs, the upper reservoir that generates quick runoff expressed by a nonlinear function and the lower reservoir that generates base flow expressed by a linear function, are included in HBV. Finally, the runoff generated from these two reservoirs is routed through a transformation function.

Xinanjiang is a rainfall–runoff model particularly developed for humid and semihumid regions by Zhao (1992). In this study, the lumped Xinanjiang model is implemented. Xinanjiang consists of four components: an evapotranspiration component represented by a model of three soil layers, including an upper layer, a lower layer, and a deep layer; a runoff generation component that considers the uneven distribution of runoff producing areas; a runoff production component separating the runoff into surface water, interflow, and groundwater; and a flow-routing component. The total runoff is finally obtained by adding the surface water, groundwater, and interflow contributions together.

f. Parameter uncertainty analysis

There are various uncertainty analysis methods like bootstrapping, Monte Carlo analysis, Bayesian model averaging, and GLUE. The uncertainty analysis method we used in this study for the assessment of parameter uncertainty is the GLUE method. It is easy to implement, and moreover, it emphasizes that there are many acceptable parameter sets that cannot be easily rejected and should be taken into account in assessing the uncertainty (Beven 2006). There are four steps in the GLUE method.

First, a large number of parameter sets based on prior parameter distributions are generated (Tang 1993). In this study, the prior distribution is represented by a uniform distribution with upper and lower bounds. The uniform distribution is recommended by Beven and Binley (1992) and is also the choice of many other researchers who applied the GLUE method. The upper and lower bounds of each parameter are based on other model applications (Zhao 1992; Seibert 1997; Perrin et al. 2003) where the potential feasible parameter values were given. Particularly, Xinanjiang was originally developed for the same river basin. The ranges for each parameter are shown in Table 3.

Second, a likelihood function is defined, a corresponding threshold value for behavioral parameter sets is chosen, and the likelihood values are calculated. The well-known Nash–Sutcliffe efficiency (NSE) coefficient is chosen as the likelihood function. NSE ranges from $-\infty$ to 1. A larger NSE means better matches between simulated data and observed data, and NSE = 1 means a perfect match between simulations and observations. A value of 0.7 is used as the threshold for determining behavioral or nonbehavioral parameter sets, which means parameter sets resulting in NSE values less than 0.7 are rejected. In total, 30 000 parameter sets are generated for each model. Behavioral parameter sets are feasible parameter sets that are able to simulate observational data with similar levels as the optimum parameter set

TABLE 2. Hydrological model description.

	GR4J	HBV	Xinanjiang
Country	France	Sweden	China
Version	Lumped	Lumped	Lumped
Numbers of parameters	4	8	15
Soil layers for evaporation	1	1	3
Flows component	Slow and quick	Base and quick	Surface, ground, and interflow

TABLE 3. Parameters of GR4J, HBV, and Xinanjiang and their ranges used for the GLUE method.

Model	Parameter	Explanation	Min	Max	Unit
GR4J	X1	Capacity of the production store	10	2000	mm
	X2	Groundwater exchange coefficient	−8	6	mm
	X3	One day ahead capacity of the routing store	10	500	mm
	X4	Time base of the unit hydrograph	0	4	day
HBV	FC	Max soil moisture capacity	100	500	mm
	LP	Soil moisture threshold for reduction of evapotranspiration	0.3	1	—
	BETA	Shape coefficient	1	5	—
	CFLUX	Max capillary flow from upper response box to soil moisture zone	1	2	mm day^{-1}
	ALFA	Measure for nonlinearity of low flow in quick runoff reservoir	0	1	—
	KF	Recession coefficient for quick flow reservoir	0.01	0.5	day^{-1}
	KS	Recession coefficient for base flow reservoir	0.001	0.1	day^{-1}
	PERC	Max flow from upper to lower response box	0	6	mm day^{-1}
Xinanjiang	SM	Areal mean free water capacity of the surface soil layer	5	50	mm
	KG	Outflow coefficient (from free water to groundwater)	0.001	0.899	—
	KI	Outflow coefficient (from free water to interflow)	0.001	0.899	
	CS	Recession constant of the surface storage	0.01	0.9	—
	CI	Recession constant of the interflow storage	0.05	0.9	—
	CG	Recession constant of the groundwater storage	0.8	0.99	—
	B	Representation of the nonuniformity of the spatial distribution	0.2	2.5	—
	UM	Soil moisture storage capacity of the upper layer	15	45	mm
	LM	Soil moisture storage capacity of the lower layer	30	80	mm
	DM	Soil moisture storage capacity of the deep layer	40	90	mm

(Beven and Freer 2001). Around 30% of the parameter sets are above the threshold.

Third, the posterior likelihood distribution for behavioral parameter sets is calculated. The behavioral parameter sets are retained. The likelihood values of these behavioral parameter sets are considered as their likelihood weights. All the weights are rescaled, so that the sum is equal to 1.

Finally, the quantiles for the predictions at every time step are estimated based on the cumulative likelihood weighted distributions. Lower 5% and upper 95% quantiles are regarded as the boundaries of 90% confidence intervals.

g. *Model calibration and validation*

The parameter ranges used in the GLUE method are listed in Table 3. The objective function for the calibration is the Nash–Sutcliffe efficiency coefficient:

$$\mathrm{NSE} = 1 - \frac{\sum_{i=1}^{T} [Q_S(i) - Q_O(i)]^2}{\sum_{i=1}^{T} [Q_O(i) - \overline{Q}_O]^2}, \tag{4}$$

where Q_S is the simulated daily discharge, Q_O is the observed daily discharge, i is the number of days, and T is the total number of days.

Meanwhile the relative volume error (RVE) is calculated as a reference indicator of the performance of the models, which is used in this study for checking the total water balance:

$$\mathrm{RVE} = 100 \times \frac{\sum_{i=1}^{T} [Q_S(i) - Q_O(i)]}{\sum_{i=1}^{T} Q_O(i)}. \tag{5}$$

GR4J, HBV, and Xinanjiang require precipitation and potential evapotranspiration (PET) as inputs. For calibration and validation purposes, the daily discharge is also needed. The parameters of the models are calibrated by the GLUE method using the observed daily precipitation and PET estimated by the Hargreaves equation from 1981 to 1990. Four, eight, and ten parameters are included in the calibration of GR4J, HBV, and Xinanjiang, respectively. The validation of the three models is carried out for the period from 1991 to 1995. The bias-corrected precipitation and temperature of PRECIS are used to drive the hydrological models to calculate the future discharges from 2011 to 2040. The historical and future discharges will be compared.

3. Results

a. *Bias-correction results*

Figure 3 shows the monthly mean precipitation and mean temperature of Jinhua River basin. The results of bias-corrected precipitation and temperature from the

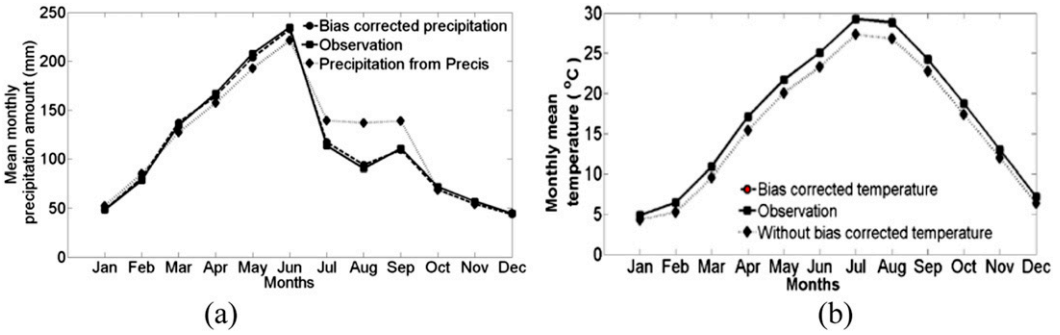

FIG. 3. Monthly mean precipitation and mean temperature for Jinhua River basin with and without bias correction.

PRECIS model are compared with the outputs of PRECIS without bias correction and observations for the baseline period from 1961 to 1990.

The smallest precipitation amount is obtained in December and is about 50 mm, which is consistent with the observations. However, compared to the observations, there are obvious biases in the uncorrected PRECIS outputs. It underestimates the precipitation for April, May, and June. The amount of observed precipitation is the largest in June with 240 mm, while the monthly mean precipitation from PRECIS is 230 mm. For July, August, and September, PRECIS significantly overestimates the observed precipitation. After bias correction, the deviation is reduced for each month and the PRECIS precipitation is closer to the observations. Figure 3b shows the temporal distribution of mean monthly temperature. The highest monthly mean temperature is close to 30°C in July. The lowest monthly mean temperature is 5°C in January. It can be seen that the uncorrected PRECIS temperature is 2°C higher than the observations on average.

b. *Performance of hydrological models*

The NSE and relative volume error values for the three models are shown in Table 4. The results of the calibration and validation show that in terms of NSE, GR4J has the best performance, with a value of 0.91 for the calibration and 0.93 for the validation. The smallest NSE value is from Xinanjiang, with 0.88 and 0.89 for calibration and validation, respectively. The performance of HBV is in between. It can be seen from RVE that GR4J overestimates the total discharge volume with a positive RVE value, while HBV underestimates the total discharge volume with a negative RVE value. For Xinanjiang, the absolute value of RVE is larger than for the other two models. Compared with other hydrological modeling studies, overestimation of the discharge by using GR4J is also found with an optimum NSE value of 0.75 (Harlan et al. 2010). Seibert (2000) used a multicriteria calibration method for HBV and suggested that the usage of efficiency mainly focused on high-flow conditions while the low-flow conditions could be better fitted by using other objective functions. Li et al. (2009) applied three versions of Xinanjiang to estimate daily runoff, and the NSE values were 0.84, 0.85, and 0.87, respectively. There is no direct relationship between NSE and RVE. In this study, the RVE is not the calibration objective function, but serves as a reference measure for the model performance.

c. *High flows in the baseline period*

The behavioral parameter sets in the three models from the GLUE method were used to estimate the parameter uncertainties expressed as 90% confidence interval (CI), which are shown as the intervals between the straight lines or the dashed lines in Fig. 4. Two sets of input data—the observed precipitation and temperature-derived PET from 1961 to 1990 and the bias-corrected precipitation and temperature-derived PET from PRECIS—are used to drive the three models. The results from two sets of input are compared. The annual maximum discharge (MHQ) was chosen to represent high flows in this study. The straight lines have been obtained by fitting a generalized extreme value (GEV) distribution to the annual maximum discharge values. Further, the observations (circles) are compared with simulated MHQ with observed inputs from optimum parameter sets (crosses).

TABLE 4. Optimum NSE and corresponding RVE of GR4J, HBV, and Xinanjiang in the Jinhua River basin for calibration and validation.

	GR4J		HBV		Xinanjiang	
	NSE	RVE (%)	NSE	RVE (%)	NSE	RVE (%)
Calibration	0.91	2.7	0.91	−2.5	0.88	−14.8
Validation	0.93	2.3	0.91	−2.1	0.89	7.8

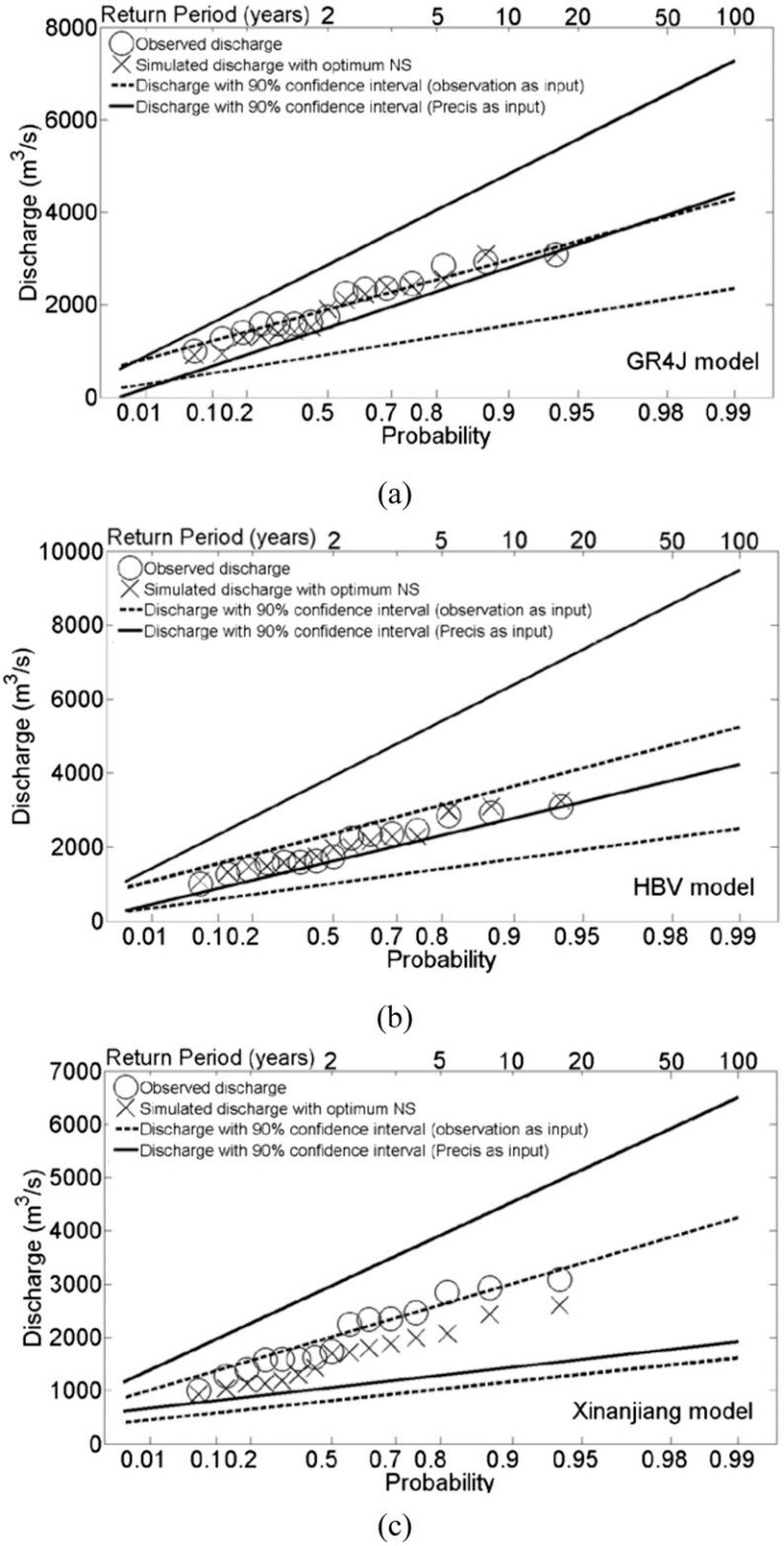

FIG. 4. The CI of high flows simulated by (a) GR4J, (b) HBV, and (c) Xinanjiang with obs and temperature and precipitation from PRECIS as input for the baseline period 1961–90.

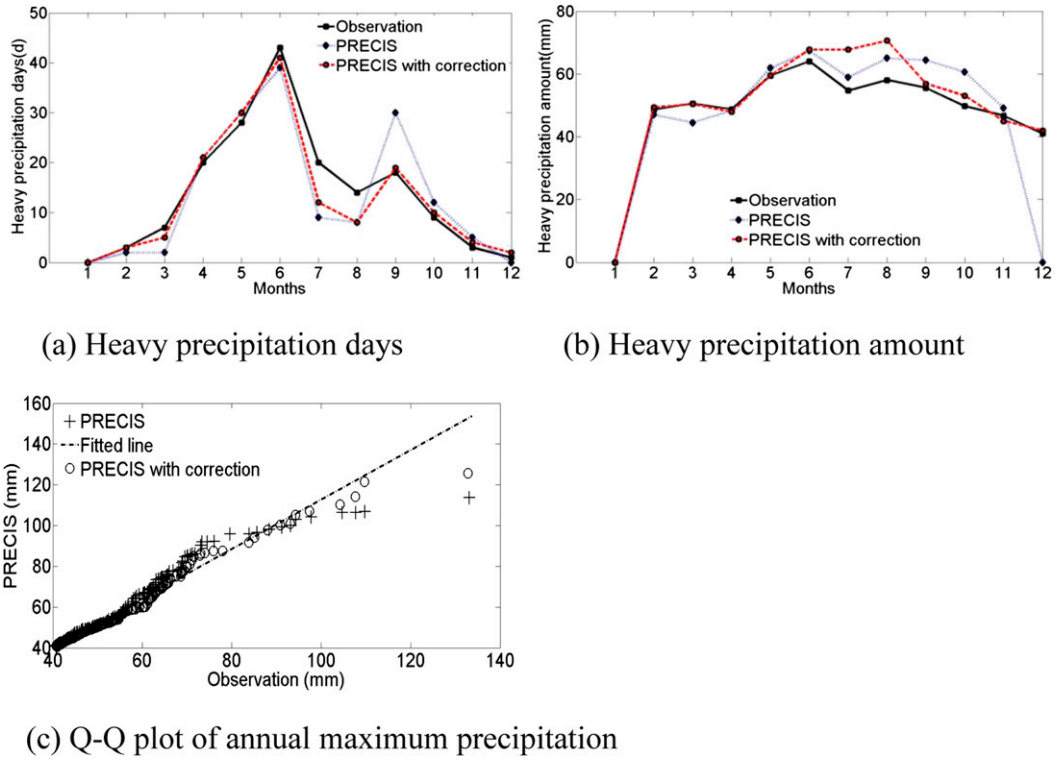

FIG. 5. Comparison of heavy precipitation and annual max precipitation between obs, PRECIS, and PRECIS with correction.

For all three models, the width of the CI becomes larger as the return period increases, which means that the parameter uncertainty increases with the discharge. In most cases, the CI covers the observed MHQ. For GR4J and HBV, the observed MHQ is close to the upper boundaries of the dashes (the CI of MHQ simulated with observed input) and also close to the lower boundaries of the straight lines (the CI of MHQ simulated with PRECIS inputs). There are obvious differences between the CI of MHQ simulated with observations and PRECIS. The CI of MHQ with PRECIS inputs is wider than that with observations for all three models. Although the precipitation and temperature of PRECIS are bias corrected and the monthly mean value is close to the observations, differences still exist in high flows when the observations and the outputs from PRECIS are used to drive the models. These differences are significant in GR4J, where the upper boundary of the CI for MHQ with observed inputs is somewhat higher than the lower boundary of the CI for MHQ with outputs from PRECIS. Xinanjiang has the largest overlapping areas in the CI of MHQ simulated with observations and PRECIS. In the study area, high flows are mainly caused by heavy precipitation over successive days. Heavy precipitation is defined as the daily precipitation being greater than the 95th percentile of precipitation on wet days during 1961–90. The amount and duration of heavy precipitation are the major aspects that affect the simulation of high flows. Figure 5 shows the days with heavy precipitation and amounts of heavy precipitation in each month for observations, PRECIS outputs, and bias-corrected PRECIS outputs. Table 5 shows the occurrences of heavy precipitation in consecutive days for the period 1961–90 for observations, PRECIS outputs, and bias-corrected PRECIS outputs. Heavy precipitation from bias-corrected PRECIS outputs resembles the observations better most of the time (see Fig. 5). However, there are fewer days with heavy precipitation, but higher heavy

TABLE 5. Occurrences of heavy precipitation in consecutive days that happened in 1961–90 for obs, PRECIS, and PRECIS with correction.

	Obs	PRECIS	PRECIS with correction
Consecutive 2 days heavy precipitation	10	33	24
Consecutive 3 days heavy precipitation	1	1	0
Consecutive 4 days heavy precipitation	0	2	2
Consecutive 5 days heavy precipitation	0	1	1

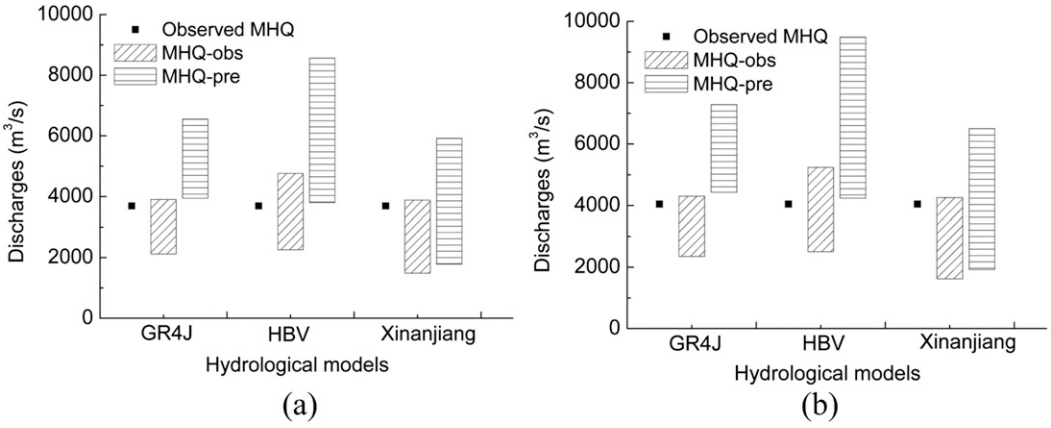

FIG. 6. The CI of extreme high flows simulated with observed and PRECIS-simulated climate as input with return periods of (a) 50 and (b) 100 years for GR4J, HBV, and Xinanjiang compared with observed high flows for the baseline period 1961–90.

precipitation amounts than observed in July and August, which may indicate larger precipitation intensity in these two months. Moreover, the annual maximum precipitation is larger for PRECIS than that for observations with the same probability. Bias correction is unable to change the duration of precipitation very effectively. In PRECIS, there are more successive days with heavy precipitation than in the observations. Heavy precipitation lasts at most for 3 days for observations in the period 1961–90, and days with heavy precipitation last at most for 5 days for PRECIS in the same period (Table 5). Therefore, there is an overestimation in MHQ even after bias correction.

The simulated MHQ (the crosses in Fig. 4) catches the observed ones for HBV and GR4J. For Xinanjiang, the simulated MHQ is smaller than the observations for all return periods with a difference ranging from 40 to 800 $m^3 s^{-1}$. The majority of observed high flows lay between the upper and lower boundary of the CI for MHQ with observed inputs. However, for all three models, they are close to the upper boundaries of the CI, which indicate that the chance of hydrological models underestimating high flows is much larger than overestimating them.

Figure 6 shows the CI of extreme high flows with a return period of 50 and 100 years simulated by GR4J, HBV, and Xinanjiang. Both the observed and PRECIS-simulated climate are used as inputs for the three models. Observed MHQs are around 3900 and 4040 $m^3 s^{-1}$ for a return period of 50 and 100 years, respectively. The CI is obviously larger for a return period of 100 years than for a return period of 50 years. The values of observed MHQ are within the range of CI estimated with the observed inputs and close to the top of the bars. The CI estimated with PRECIS inputs are wider and obviously higher and for all three models similar results are obtained, which indicate that the input data has a dominant impact on the discharges. Extreme high flows tend to be underestimated using observed data as inputs and overestimated if the PRECIS data are used as inputs for the model. In general, the MHQ has a larger uncertainty range with PRECIS data as inputs than with observations as inputs.

For the CI estimated with the observations, it shows that uncertainties expressed as 90% confidence intervals are the largest for HBV, with 2200–4800 and 2500–5250 $m^3 s^{-1}$ for 50- and 100-yr return periods. Uncertainties are the smallest for GR4J, with 2100–3900 and 2350–4300 $m^3 s^{-1}$, respectively. The CIs estimated with PRECIS input are 3900–6600, 3700–8600, and 1800–5900 $m^3 s^{-1}$ for GR4J, HBV, and Xinanjiang, respectively, for the 50-yr return period. For the 100-yr return period, they are 4400–7300, 4200–9500, and 2000–6500 $m^3 s^{-1}$, respectively.

d. Uncertainties in future projected high flows

In Fig. 7, three graphs show the high flows under scenarios A1B, A2, and B2 as a function of their return periods for the time period 2011–40 and the baseline period. For all three models, it is remarkable to notice that compared to the baseline, there would be a slight decrease of high flows in the future for a return period of 5 years. The decrease in high flows becomes obvious over the 5-yr return period for all scenarios. When the return periods are above 5 years, the high flows under scenario A2 are smaller than those under scenarios A1B and B2 for all three hydrological models in most cases, which means under scenario A2 future high flows with higher return periods would decline more than under scenarios A1B and B2.

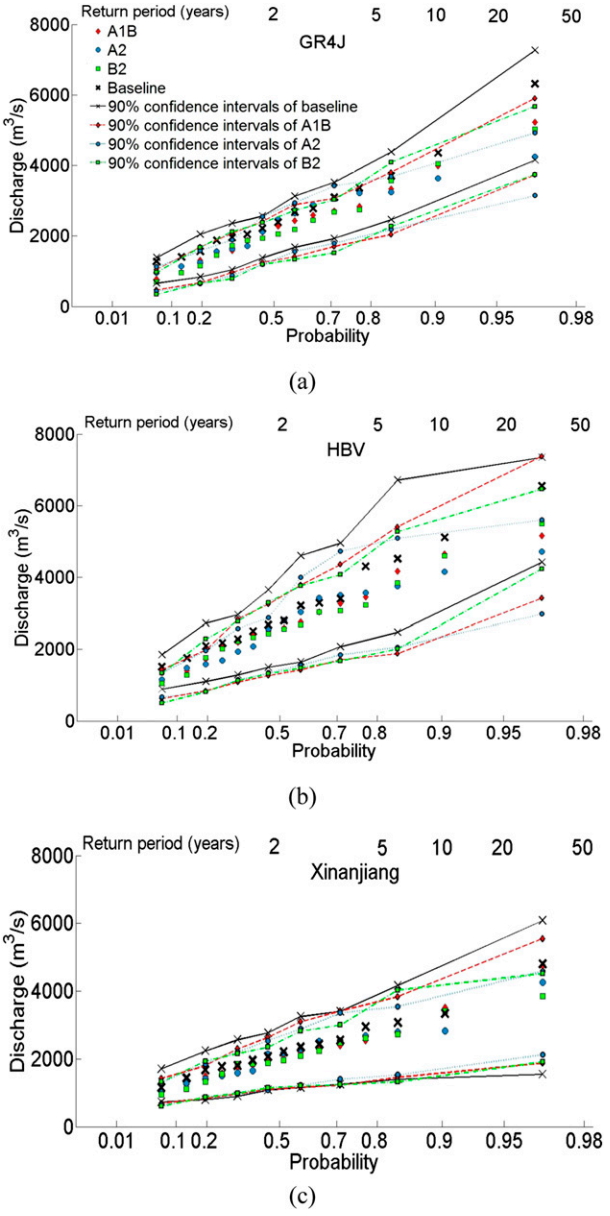

FIG. 7. High flows with uncertainties as a function of return period simulated by (a) GR4J, (b) HBV, and (c) Xinanjiang under scenarios A1B, B2, and A2 in the baseline period and in the period 2011–40.

Furthermore, it can be seen that the CI becomes wider with increasing return periods. For GR4J, the ranges of the uncertainty in high flows for the baseline and the future scenarios are similar. Both the upper and lower limits of the CI in the baseline are the largest, followed by the A1B and B2 scenarios, and the A2 scenario has smaller upper and lower limits of the CI. It illustrates that the high flows tend to decrease under all three scenarios, but the uncertainty range does not clearly change. For HBV, there is a similar simulation as GR4J, high flows decrease under three scenarios, and the largest decrease of high flows is under scenario A2. For Xinanjiang, the lower limits of the CI are similar while the upper limits differ for the baseline and the future scenarios. The upper limits of the CI are the highest for the baseline and are followed by scenarios A1B, B2, and A2 in sequence from high to low. It is apparent that although there are differences in the CI of different scenarios, the markers for all scenarios are within the ranges of the straight lines derived from the parameter uncertainty. This indicates that the uncertainties of the parameters are larger than those of the scenarios. The ranges of differences in MHQ due to different scenarios for return periods of 1–30 years are 25–970, 100–780, and 60–920 $m^3 s^{-1}$ for GR4J, HBV, and Xinanjiang, respectively.

Figure 8 illustrates the MHQ with uncertainties from different models under scenarios A1B, A2, B2, and the baseline period. For the baseline period and all scenarios, the MHQs estimated by the three models are close to each other when the return period is small and the differences become larger with increasing return periods. In the baseline period and all scenarios, the MHQ from HBV is the largest for almost all return periods and Xinanjiang has the lowest MHQ. The ranges of differences in MHQ due to the different hydrological models for return periods of 1–30 years are 240–1750, 270–1380, 190–1350, and 260–1650 $m^3 s^{-1}$ for the baseline period and scenarios A1B, A2, and B2, respectively. The ranges of differences in MHQ are calculated by the lowest and highest MHQ from a 1–30-yr return period. The mean uncertainty range of the MHQ from parameters, models, and scenarios is also shown in Table 6. Compared to the ranges of the difference of MHQ due to the scenarios, the difference of the MHQ due to models is larger for a corresponding return period. It indicates that the uncertainty of the model structure is larger than that of scenarios. Further, it is remarkable that the markers for all models are also covered by the confidence interval due to parameter uncertainty (as shown in Fig. 7), which means the uncertainties of the parameters are larger than that of the model structures. Therefore, in this study, the major source of uncertainty in high flows is from parameters, followed by the hydrological model structure, and uncertainties from the scenarios have the smallest uncertainty contribution. This conclusion is in accordance with the conclusion of Bastola et al. (2011), who found that the role of the hydrological model structure is remarkably large, but is different from the results of Li et al. (2010), who found out that the parameter uncertainty contributes a relatively small part to the model output uncertainty when applying the bootstrapping method to the SWAT model.

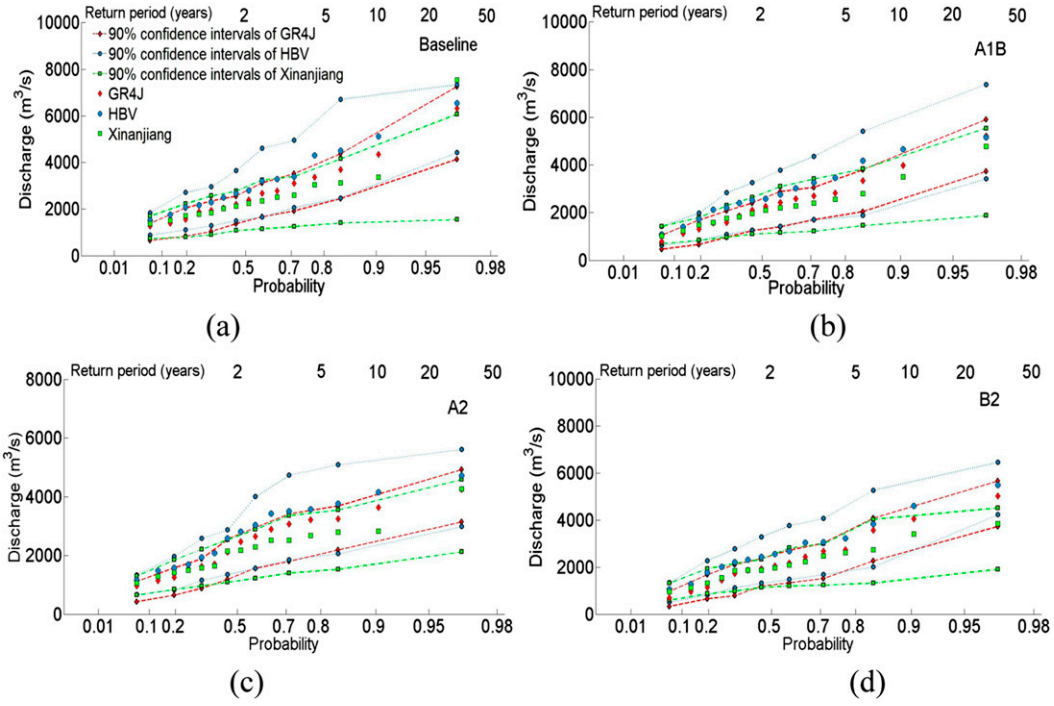

FIG. 8. High flows with uncertainties as a function of return period simulated for (a) the baseline period 1961–90 and under scenarios (b) A1B, (c) A2, and (d) B2 in the period 2011–40 by GR4J, HBV, and Xinanjiang.

The difference is that in the work of Li et al. (2010), the model was recalibrated each time after the residuals were added to the simulation results. As the residuals were assumed to be independent in time, the deviation of the recalibrated parameter set from the original one would be limited.

There are some common characteristics in the four scenarios in Fig. 8. First, the upper boundary of the CI of the MHQ for HBV is the highest, which means that it is more likely to predict a higher MHQ with HBV. Additionally, GR4J has a smaller CI than the other two models, which illustrates that the parameter uncertainty in GR4J is the smallest. Furthermore, most of the markers are not in the middle of the CI but are closer to the upper boundaries for three hydrological models, so there is a larger chance to underestimate rather than overestimate the MHQ under the climate change.

We simulated the MHQ with uncertainty using three hydrological models and extrapolated it to return periods of 50 and 100 years under the scenarios A1B, A2, and B2, as shown in Fig. 9. Obviously, the CIs are wider for a return period of 100 years than for a return period of 50 years. For all scenarios, GR4J has the smallest CI, followed by Xinanjiang, and the largest is from HBV (Table 7). This order is in accordance with the baseline period. Xinanjiang gives the smallest estimation of MHQ for both return periods.

4. Discussion

It is widely acknowledged that climate change uncertainties are much larger when feeding into rainfall–runoff models than the hydrological uncertainties within the models themselves. The largest uncertainties in

TABLE 6. The uncertainty range of the MHQ from parameters, models, and scenarios in 5-, 10-, 20-, and 30-yr return periods.

Return periods (years)	Parameters ($m^3 s^{-1}$)			Models ($m^3 s^{-1}$)			Scenarios ($m^3 s^{-1}$)		
	Upper bounds	Lower bounds	Difference	Upper bounds	Lower bounds	Difference	Upper bounds	Lower bounds	Difference
5	3953	1747	2206	3370	2795	975	3236	3038	198
10	4710	2143	2567	4632	3277	1355	4070	3540	530
20	5088	2288	2800	4849	4071	778	4410	4128	282
30	5626	3022	2604	5748	4899	949	5165	4274	891

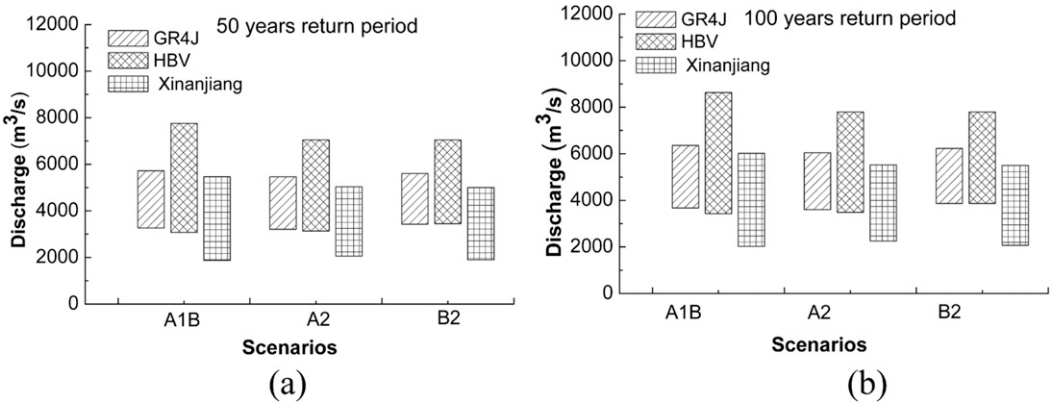

FIG. 9. CI of MHQ with a return period of (a) 50 and (b) 100 years under scenarios A1B, A2, and B2 as estimated by GR4J, HBV, and Xinanjiang.

projected streamflow under climate change come from uncertainties in climate change emissions scenarios (Houghton et al. 2001), but the conclusion is not suitable for all cases because of the different regional climates and possible changes that may take place under the future emissions scenarios. The results of this study show that for the study area, the uncertainties from the hydrological model structures are larger than those from emissions scenarios. Furthermore, the uncertainty from parameters in hydrological models contributes the most to the model output uncertainty. Wilby and Harris (2006) studied the uncertainty in future low flows and concluded that the hydrological model structure uncertainty was the most important source, followed by the parameter uncertainty and the emissions scenario uncertainty. Moreover, different GCMs and downscaling methods (including RCMs) could also cause differences in the order of significant uncertainty sources, which are not, however, investigated in this study. There are also uncertainties related to high flows with different return periods because of the limited length of discharge time series and the extrapolation method. Figure 10 shows the uncertainties in high flows with 50- and 100-yr return periods from extrapolation method by GEV distribution. The bootstrap method is applied to sample 1000 sets from 30 years of annual maximum discharges in the baseline period from three hydrological models. Then, the GEV distribution is fitted to each sampling set and the uncertainty in high flows with 50- and 100-yr return periods due to extrapolation is estimated. The uncertainty ranges of high flows due to extrapolation are between 1000 and 2000 $m^3 s^{-1}$ depending on the models and return periods, but they are smaller than those from parameters of the hydrological models. In general, a more thorough uncertainty analysis is recommended for further application of this study to, for instance, climate adaptation purposes in water management.

In this study, the most important uncertainty source is from hydrological parameters. The parameter uncertainties are related to the number of parameters for calibration, the calibration ranges of each parameter, and also the threshold defined for the behavioral parameter sets. Jin et al. (2010) used 0.6 and 0.8 as thresholds for the Nash–Sutcliffe coefficient and concluded that lower threshold values may result in a wider uncertainty interval of the posterior distribution of parameters and a wider confidence interval of model uncertainty. Since it is not possible to eliminate parameter uncertainties at present and the large influence of parameter uncertainty on high flows is evident, it is recommended that parameter uncertainty should be taken into account in water resource management when hydrological models are applied. The results also reveal that parameter uncertainties of GR4J are the smallest, followed by Xinanjiang and HBV. Since the threshold for the behavioral parameter sets is equal for the three models, it is possible that the number of calibrated parameters and parameter ranges contribute to the result that GR4J has the smallest uncertainty.

TABLE 7. The range of CIs for GR4J of MHQ with a return period of 50 and 100 years under scenarios A1B, A2, and B2 from three models.

Return periods (years)	Scenarios	GR4J ($m^3 s^{-1}$)	HBV ($m^3 s^{-1}$)	Xinanjiang ($m^3 s^{-1}$)
50	A1B	2450	4861	3596
	A2	2248	3912	2975
	B2	2173	3592	3102
100	A1B	2687	5201	3393
	A2	2448	4310	3274
	B2	2362	3927	3430

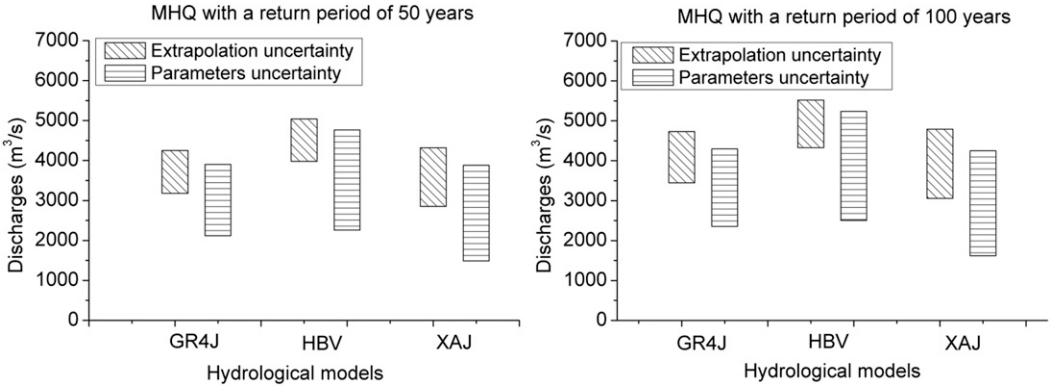

FIG. 10. Comparison of uncertainty ranges of extrapolation and parameters in the models.

In this study, only one GCM and one RCM were applied for the three hydrological models. Therefore, the uncertainty might be underestimated without considering multiple GCMs or RCMs. Teutschbein and Seibert (2010) stressed that multimodel approaches in rainfall–runoff simulation are useful for climate change impact assessment. They also suggested that when applying RCMs for hydrological impact studies, ensembles of RCMs should be used because of model biases and intermodel variability. Sometimes, the number of GCMs, RCMs, and scenarios are limited. One possible solution to the limited number of the RCMs and GCMs would be using the imprecise cumulative distribution function (CDF) method. This is a nonparametric method used to determine the probability distribution function, which not only contains the CDFs generated with all available GCMs but also accounts for the uncertainties from the missing ones (Ghosh and Mujumdar 2009).

The methods and findings presented here could be useful when applying the PRECIS data in other hydrological models or when using the same hydrological models. The next step would be to incorporate different GCMs and RCMs in the analysis of uncertainty for high flows.

5. Conclusions

In this paper, the impacts of uncertainties from future emissions scenarios, hydrological model structures, and parameters on high flows were investigated using the regional climate model PRECIS. The temperature and precipitation from PRECIS were bias corrected and then applied as inputs for the hydrological models GR4J, HBV, and Xinanjiang. The Jinhua River basin in eastern China was chosen as a case study area. The GLUE method was used to calibrate the hydrological models and to quantify the parameter uncertainties of the three hydrological models.

In Jinhua River basin, the largest bias of PRECIS is in the overestimation of the precipitation in July, August, and September. PRECIS overestimated the observed temperature with about 2°C all year round. After bias correction, the temporal distributions of monthly precipitation and temperature were closer to the observations, but there is still some bias, especially in the heavy precipitation. Higher precipitation intensities can be observed in July and August, and the number of successive days with heavy precipitation is also larger for PRECIS than that for the observations. The bias-corrected temperature and precipitation and the observed temperature and precipitation were used to drive the hydrological models to simulate high flows in the baseline period. The results showed that because of the bias in the simulation of heavy precipitation in the baseline period, high flows driven by PRECIS are likely to be overestimated in the future. For a return period of 100 years, the uncertainties in high flows were larger with PRECIS inputs than observed inputs. The behavior of the three hydrological models was similar in the sense that they tended to underestimate high flows.

The 90% confidence intervals became larger with increasing return periods under all emissions scenarios. For all three hydrological models, the high flows tend to decrease under scenarios A1B, A2, and B2, but the uncertainty ranges do not change noticeably. The uncertainty ranges of MHQ due to different scenarios for return periods of 1–30 years are 25–970, 100–780, and 60–920 $m^3 s^{-1}$ for GR4J, HBV, and Xinanjiang, respectively.

High flows simulated by HBV were the largest, followed by GR4J, and Xinanjiang had the smallest high flows. The largest uncertainty was observed in HBV, GR4J had the smallest uncertainty, and Xinanjiang was in between. The uncertainty ranges in MHQ from models for return periods of 1–30 years were 240–1750, 270–1380, 190–1350, and 260–1650 $m^3 s^{-1}$ for the baseline

period and scenarios A1B, A2, and B2, respectively. The major sources of uncertainty in this study were from the parameters, followed by uncertainties from the scenarios, and the hydrological model structure caused the smallest uncertainty. It should be noted that in the GLUE method, the choice of threshold and parameter ranges is subjective. Also, the parameter ranges may be enlarged by bias correction, but the forcing from PRECIS is still not accurate enough (see Fig. 6). The bias from PRECIS was not avoidable until now, and the choice of parameter ranges was made based on many previous studies. Therefore, the conclusion that the parameter uncertainty is the main source is conditional on these subjective matters. The uncertainty analysis is important because it improves the understanding of the major problems and hence may support decision and policy making in water resources management.

Acknowledgments. This study is financially supported by the International Science and Technology Cooperation Program of China (Project 2010DFA24320) and the Nature Science Foundation of China (Projects 51379183 and 50809058). Other support from the National Climate Center of China Meteorological Administration and Bureau of Hydrology in Zhejiang Province are acknowledged for providing data for this study. Last but not least, the valuable comments and suggestions from the editor and two anonymous reviewers are greatly appreciated.

REFERENCES

Akhtar, M., N. Ahmad, and M. J. Booij, 2008: The impact of climate change on the water resources of Hindukush–Karakorum–Himalaya region under different glacier coverage scenarios. *J. Hydrol.,* **355,** 148–163, doi:10.1016/j.jhydrol.2008.03.015.

——, ——, and ——, 2009: Use of regional climate model simulations as input for hydrological models for the Hindukush–Karakorum–Himalaya region. *Hydrol. Earth Syst. Sci.,* **13,** 1075–1089, doi:10.5194/hess-13-1075-2009.

Arnell, N. W., 2003: Effects of IPCC SRES* emissions scenarios on river runoff: A global perspective. *Hydrol. Earth Syst. Sci.,* **7,** 619–641, doi:10.5194/hess-7-619-2003.

——, D. A. Hudson, and R. G. Jones, 2003: Climate change scenarios from a regional climate model: Estimating change in runoff in southern Africa. *J. Geophys. Res.,* **108,** 4519, doi:10.1029/2002JD002782.

Bastola, S., C. Murphy, and J. Sweeney, 2011: The role of hydrological modelling uncertainties in climate change impact assessments of Irish river catchments. *Adv. Water Resour.,* **34,** 562–576, doi:10.1016/j.advwatres.2011.01.008.

Bauwens, A., C. Sohier, and A. Degré, 2011: Hydrological response to climate change in the Lesse and the Vesdre catchments: Contribution of a physically based model (Wallonia, Belgium). *Hydrol. Earth Syst. Sci.,* **15,** 1745–1756, doi:10.5194/hess-15-1745-2011.

Bell, J. L., L. C. Sloan, and M. A. Snyder, 2004: Regional changes in extreme climatic events: A future climate scenario. *J. Climate,* **17,** 81–87, doi:10.1175/1520-0442(2004)017<0081:RCIECE>2.0.CO;2.

Bergström, S., 1976: Development and application of a conceptual runoff model for Scandinavian catchments. SMHI Rep. RHO 7, 133 pp.

——, 1992: The HBV model—Its structure and applications. SMHI Rep. RH 4, 35 pp.

Beven, K., 2006: A manifesto for the equifinality thesis. *J. Hydrol.,* **320,** 18–36, doi:10.1016/j.jhydrol.2005.07.007.

——, and A. Binley, 1992: The future of distributed models: Model calibration and uncertainty prediction. *Hydrol. Processes,* **6,** 279–298, doi:10.1002/hyp.3360060305.

——, and J. Freer, 2001: Equifinality, data assimilation, and uncertainty estimation in mechanistic modelling of complex environmental systems using the GLUE methodology. *J. Hydrol.,* **249,** 11–29, doi:10.1016/S0022-1694(01)00421-8.

——, ——, B. Hankin, and K. Schulz, 2000: The use of generalised likelihood measures for uncertainty estimation in high order models of environmental systems. *Nonlinear and Non-stationary Signal Processing,* W. J. Fitzgerald et al., Eds., Cambridge University Press, 115–151.

Booij, M., 2005: Impact of climate change on river flooding assessed with different spatial model resolutions. *J. Hydrol.,* **303,** 176–198, doi:10.1016/j.jhydrol.2004.07.013.

Boorman, D. B., and C. Sefton, 1997: Recognising the uncertainty in the quantification of the effects of climate change on hydrological response. *Climatic Change,* **35,** 415–434, doi:10.1023/A:1005372407881.

Buytaert, W., M. Vuille, A. Dewulf, R. Urrutia, A. Karmalkar, and R. Celleri, 2010: Uncertainties in climate change projections and regional downscaling in the tropical Andes: Implications for water resources management. *Hydrol. Earth Syst. Sci.,* **14,** 1247–1258, doi:10.5194/hess-14-1247-2010.

Driessen, T., R. Hurkmans, W. Terink, P. Hazenberg, P. Torfs, and R. Uijlenhoet, 2010: The hydrological response of the Ourthe catchment to climate change as modelled by the HBV model. *Hydrol. Earth Syst. Sci.,* **14,** 651–665, doi:10.5194/hess-14-651-2010.

Edijatno, N. D. O. N., X. Yang, Z. Makhlouf, and C. Michel, 1999: GR3J: A daily watershed model with three free parameters. *Hydrol. Sci. J.,* **44,** 263–277, doi:10.1080/02626669909492221.

Ghosh, S., and P. Mujumdar, 2009: Climate change impact assessment: Uncertainty modeling with imprecise probability. *J. Geophys. Res.,* **114,** D18113, doi:10.1029/2008JD011648.

Gordon, C., and Coauthors, 2000: The simulation of SST, sea ice extents and ocean heat transports in a version of the Hadley Centre coupled model without flux adjustments. *Climate Dyn.,* **16,** 147–168, doi:10.1007/s003820050010.

Gosain, A. K., S. Rao, and A. Arora, 2011: Climate change impact assessment of water resources of India. *Curr. Sci.,* **101,** 356–371.

Hannaford, J., and T. J. Marsh, 2008: High flow and flood trends in a network of undisturbed catchments in the UK. *Int. J. Climatol.,* **28,** 1325–1338, doi:10.1002/joc.1643.

Hargreaves, G. H., and Z. A. Samani, 1983: Estimating potential evapotranspiration. *J. Irrig. Drain. Div.,* **108,** 225–230.

Harlan, D., M. Wangsadipura, and C. M. Munajat, 2010: Rainfall–runoff modeling of Citarum Hulu River basin by using GR4J. *Proc. World Congress on Engineering 2010,* London, United

Kingdom, International Association of Engineers, 1607–1611.

Houghton, J. T., Y. Ding, D. J. Griggs, M. Noguer, P. J. van der Linden, X. Dai, K. Maskell, and C. A. Johnson, Eds., 2001: *Climate Change 2001: The Scientific Basis.* Cambridge University Press, 881 pp.

Jin, X., C. Y. Xu, Q. Zhang, and V. Singh, 2010: Parameter and modeling uncertainty simulated by GLUE and a formal Bayesian method for a conceptual hydrological model. *J. Hydrol.,* **383,** 147–155, doi:10.1016/j.jhydrol.2009.12.028.

Jones, R. G., M. Noguer, D. C. Hassell, D. Hudson, S. S. Wilson, G. J. Jenkins, and J. F. B. Mitchell 2004: Generating high resolution climate change scenarios using PRECIS. Met Office Hadley Centre Rep., 40 pp.

Jones, R. N., F. H. S. Chiew, W. C. Boughton, and L. Zhang, 2006: Estimating the sensitivity of mean annual runoff to climate change using selected hydrological models. *Adv. Water Resour.,* **29,** 1419–1429, doi:10.1016/j.advwatres.2005.11.001.

Kay, A. L., H. N. Davies, V. A. Bell, and R. G. Jones, 2009: Comparison of uncertainty sources for climate change impacts: Flood frequency in England. *Climatic Change,* **92,** 41–63, doi:10.1007/s10584-008-9471-4.

Kerkhoven, E., and T. Y. Gan, 2013: Differences in the potential hydrologic impact of climate change to the Athabasca and Fraser River basins of Canada with and without considering shifts in vegetation patterns induced by climate change. *J. Hydrometeor.,* **14,** 963–976, doi:10.1175/JHM-D-12-011.1.

Leander, R., T. A. Buishand, B. J. J. M. van den Hurk, and M. J. M. de Wit, 2008: Estimated changes in flood quantiles of the river Meuse from resampling of regional climate model output. *J. Hydrol.,* **351,** 331–343, doi:10.1016/j.jhydrothrl.2007.12.020.

Li, H., Y. Zhang, F. H. S. Chiew, and S. Xu, 2009: Predicting runoff in ungauged catchments by using Xinanjiang model with MODIS leaf area index. *J. Hydrol.,* **370,** 155–162, doi:10.1016/j.jhydrol.2009.03.003.

Li, Z., Q. Shao, Z. Xu, and X. Cai, 2010: Analysis of parameter uncertainty in semi-distributed hydrological models using bootstrap method: A case study of SWAT model applied to Yingluoxia watershed in northwest China. *J. Hydrol.,* **385,** 76–83, doi:10.1016/j.jhydrol.2010.01.025.

Lindström, G., B. Johansson, M. Persson, M. Gardelin, and S. Bergström, 1997: Development and test of the distributed HBV-96 hydrological model. *J. Hydrol.,* **201,** 272–288, doi:10.1016/S0022-1694(97)00041-3.

Middelkoop, H., and Coauthors, 2001: Impact of climate change on hydrological regimes and water resources management in the Rhine basin. *Climatic Change,* **49,** 105–128, doi:10.1023/A:1010784727448.

Najafi, M. R., H. Moradkhani, and I. W. Jung, 2011: Assessing the uncertainties of hydrologic model selection in climate change impact studies. *Hydrol. Processes,* **25,** 2814–2826, doi:10.1002/hyp.8043.

Nakićenović, N., and R. Swart, Eds., 2000: *Special Report on Emissions Scenarios.* Cambridge University Press, 570 pp.

New, M., and M. Hulme, 2000: Representing uncertainty in climate change scenarios: A Monte-Carlo approach. *Integr. Assess.,* **1,** 203–213, doi:10.1023/A:1019144202120.

Pachauri, R. K., and A. Reisinger, Eds., 2007: *Climate Change 2007: Synthesis Report.* Intergovernmental Panel on Climate Change, 104 pp.

Parrish, M. A., H. Moradkhani, and C. M. DeChant, 2012: Toward reduction of model uncertainty: Integration of Bayesian model averaging and data assimilation. *Water Resour. Res.,* **48,** W03519, doi:10.1029/2011WR011116.

Perrin, C., C. Michel, and V. Andreassian, 2003: Improvement of a parsimonious model for streamflow simulation. *J. Hydrol.,* **279,** 275–289, doi:10.1016/S0022-1694(03)00225-7.

Raftery, A. E., T. Gneiting, F. Balabdaoui, and M. Polakowski, 2005: Using Bayesian model averaging to calibrate forecast ensembles. *Mon. Wea. Rev.,* **133,** 1155–1174, doi:10.1175/MWR2906.1.

Raje, D., and P. Mujumdar, 2010: Constraining uncertainty in regional hydrologic impacts of climate change: Nonstationarity in downscaling. *Water Resour. Res.,* **46,** W07543, doi:10.1029/2009WR008425.

Rebora, N., and Coauthors, 2013: Extreme rainfall in the Mediterranean: What can we learn from observations? *J. Hydrometeor.,* **14,** 906–922, doi:10.1175/JHM-D-12-083.1.

Refsgaard, J. C., J. P. van der Sluijs, J. Brown, and P. van der Keur, 2006: A framework for dealing with uncertainty due to model structure error. *Adv. Water Resour.,* **29,** 1586–1597, doi:10.1016/j.advwatres.2005.11.013.

Seibert, J., 1997: Estimation of parameter uncertainty in the HBV model. *Nord. Hydrol.,* **28,** 247–262.

——, 2000: Multi-criteria calibration of a conceptual runoff model using a genetic algorithm. *Hydrol. Earth Syst. Sci.,* **4,** 215–224, doi:10.5194/hess-4-215-2000.

Tang, B., 1993: Orthogonal array-based Latin hypercubes. *J. Amer. Stat. Assoc.,* **88,** 1392–1397, doi:10.1080/01621459.1993.10476423.

Teutschbein, C., and J. Seibert, 2010: Regional climate models for hydrological impact studies at the catchment scale: A review of recent modeling strategies. *Geogr. Compass,* **4,** 834–860, doi:10.1111/j.1749-8198.2010.00357.x.

Tian, Y., Y.-P. Xu, and X.-J. Zhang, 2013: Assessment of climate change impacts on river high flows through comparative use of GR4J, HBV and Xinanjiang models. *Water Resour. Manage.,* **27,** 2871–2888, doi:10.1007/s11269-013-0321-4.

Ueyama, H., S. Adachi, and F. Kimura, 2010: Compilation method for 1 km grid data of monthly mean air temperature for quantitative assessments of climate change impacts. *Theor. Appl. Climatol.,* **101,** 421–431, doi:10.1007/s00704-009-0228-4.

Vrugt, J. A., H. V. Gupta, L. A. Bastidas, W. Bouten, and S. Sorooshian, 2003: Effective and efficient algorithm for multiobjective optimization of hydrologic models. *Water Resour. Res.,* **39,** 1214, doi:10.1029/2002WR001746.

Wen, K. G., G. Y. Xi, and W. N. Xu, 2006: *Dictionary of Chinese Meteorological Disaster* (in Chinese). China Meteorology Press, 287 pp.

Wigley, T., P. Jones, K. Briffa, and G. Smith, 1990: Obtaining subgrid-scale information from coarse-resolution general circulation model output. *J. Geophys. Res.,* **95,** 1943–1953, doi:10.1029/JD095iD02p01943.

Wilby, R. L., and I. Harris, 2006: A framework for assessing uncertainties in climate change impacts: Low-flow scenarios for the River Thames, UK. *Water Resour. Res.,* **42,** W02419, doi:10.1029/2005WR004065.

——, H. Hassan, and K. Hanaki, 1998: Statistical downscaling of hydrometeorological variables using general circulation model output. *J. Hydrol.,* **205,** 1–19, doi:10.1016/S0022-1694(97)00130-3.

——, L. E. Hay, and G. H. Leavesley, 1999: A comparison of downscaled and raw GCM output: Implications for climate change scenarios in the San Juan River basin, Colorado. *J. Hydrol.,* **225,** 67–91, doi:10.1016/S0022-1694(99)00136-5.

——, C. W. Dawson, and E. M. Barrow, 2002: SDSM—A decision support tool for the assessment of regional climate change

impacts. *Environ. Modell. Software,* **17,** 145–157, doi:10.1016/S1364-8152(01)00060-3.

Wood, A. W., E. P. Maurer, A. Kumar, and D. P. Lettenmaier, 2002: Long-range experimental hydrologic forecasting for the eastern United States. *J. Geophys. Res.,* **107,** 4429, doi:10.1029/2001JD000659.

Xu, Y.-P., X. Zhang, and Y. Tian, 2012: Impact of climate change on 24-h design rainfall depth estimation in Qiantang River basin, east China. *Hydrol. Processes,* **26,** 4067–4077, doi:10.1002/hyp.9210.

——, ——, Q. Ran, and Y. Tian, 2013: Impact of climate change on hydrology of upper reaches of Qiantang River basin, east China. *J. Hydrol.,* **483,** 51–60, doi:10.1016/j.jhydrol.2013.01.004.

Zhang, Q., V. P. Singh, P. Sun, X. Chen, Z. Zhang, and J. Li, 2011: Precipitation and streamflow changes in China: Changing patterns, causes and implications. *J. Hydrol.,* **410,** 204–216, doi:10.1016/j.jhydrol.2011.09.017.

Zhao, R.-J., 1992: The Xinanjiang model applied in China. *J. Hydrol.,* **135,** 371–381, doi:10.1016/0022-1694(92)90096-E.